



Data-driven buckling capacity prediction of normal- and high-strength steel hollow structural section columns

Hyeyoung Koh¹, Hannah B. Blum²

Abstract

The use of high-strength steel has been increasing in the steel construction industry due to its high strength-to-weight ratio. Currently, high-strength steel columns are designed by equations that were developed for normal-strength steel, which has shown to result in conservative predictions for high-strength steel columns. Moreover, the current version of AISC 360 is limited to hollow structural sections (HSS) with steel grades up to 485 MPa. This study establishes a data-driven design approach for HSS columns that addresses a range of steel grades up to 960 MPa, residual stresses, geometric imperfections, and geometry including member and element slenderness. An extensive database for square and rectangular HSS columns is constructed from the existing literature containing both experimental and numerical research. Conventional interpolation and newer machine learning methods were adopted to examine the buckling strength estimation. The predictions derived from the proposed data-driven model were compared with the capacities estimated by AISC 360 to examine the accuracy of current design rules for HSS columns. The data was divided into groups to study the effect of factors on the design prediction accuracy, including (1) normal- vs. high-strength grades and (2) hot-rolled vs. cold-formed sections. In addition, the database and all analysis methods are coded in a user-friendly computational notebook format for ease of use and saved in the open-source repository so future researchers and users can update and modify the analysis as future data is generated.

1. Introduction

The advances in computational capabilities have enabled access to comprehensive data that includes a large number of observations and parameters. Structural engineers can exploit data to make use of large amounts of data acquired through physical experiments and advanced technical computing systems. To efficiently perform operations for tasks using the data, it is necessary to design a data structure, which is a storage that is used to store and organize data. The data structure is a way of arranging data on a computer so that it can be accessed and updated efficiently by users. However, the industry has looked for help from specialists to handle a vast amount of field data

¹Postdoctoral Researcher, formerly PhD Candidate, University of Wisconsin-Madison, <hyeyoung.koh@wisc.edu>

²Assistant Professor and Alain H. Peyrot Fellow, University of Wisconsin-Madison, <hannah.blum@wisc.edu>

for data review and mapping data, which can be time- and resource-consuming. Moreover, structural engineering has not taken full advantage of advancements in data analytics compared with other civil engineering subdisciplines (El-Dakhakhni 2021). Introducing programming language written analysis methods and data structures for structural design can advance data analytics in the structural engineering community.

Data-driven design approaches such as interpolation and regression have broad applications for predictive analysis using the data. However, interpolation and regression are theoretically derived from univariate prediction, therefore they become challenging when large data is applied while maintaining tractable computational complexity (Lux et al. 2021). Recently, machine learning (ML) techniques have shown significant advantages in estimating underlying complex relationships of parameters and could help the structural design industry benefit from the vast quantities of available data. ML has been implemented to predict responses of steel structural components (Pala 2006; Pu and Mesbahi 2006; Sheidaii and Bahraminejad 2012; Kumar and Yadav 2013; Abambres et al. 2018; Xu et al. 2021; Fang et al. 2021; Dai et al. 2022), which have demonstrated the ability to improve the regression accuracy of capacity prediction of steel components. However, most of the studies listed above considered either only experimental or numerical results to predict the structural responses while both physical testing and numerical results can be used for structural analysis and design per multiple steel design codes (AISC 360 2016; Eurocode 3 2014; AS 4100 1998; AS/NZS 4600 2018; CSA S16 2019).

To introduce a data structure for structural design and data-driven models using a database that includes both experimental and numerical data, this study explores the buckling capacity of square and rectangular hollow section (SHS and RHS) columns. Hollow sections are widely used as structural elements in buildings and other structures due to their structural efficiency coming from a high strength-to-weight ratio, therefore a large data from the literature is available. The predominant manufacturing processes of SHS and RHS members are hot-rolling, cold-forming, or welding four steel plates into a box shape.

Design rules for SHS and RHS members in compression are codified in the US specification for structural steel buildings AISC 360 (2016). Experimental and numerical results for various cross-section types and sizes with geometric imperfections were incorporated to build the buckling curves given in the codified provisions. AISC 360 (2016) has a single buckling curve based on the numerical results of columns with an initial out-of-straightness, which were studied by Tide (1985), Bjorhovde (1988), and Galambos (1998). Although the codified provisions have been broadly used in the structural steel industry, the accuracy and efficiency of the design rules can be improved by addressing several challenges; (1) Although high-strength steel grades have been available due to the advancement of steel manufacturing technology in recent years, the design rules for them are a simple extension of those for normal-strength steels and do not directly address the influence of material yield strength. AISC 360 (2016) has limited provisions for hollow sections with steel grades greater than 485 MPa. A predictive model that addresses a wide spectrum of steel grades could address this issue. (2) Formation methods are not incorporated into the design rules and cold-formed hollow sections follow the design rules for hot-rolled hollow sections. The test capacity of high-strength steel columns (Sedlacek et al. 1999; Ma et al. 2016; Wang and Gardner 2017; Meng and Gardner 2020) predicted by the existing design rules were shown to

be overly conservative, which may generate an inefficient and thus costly design. Moreover, it was reported that the AISC method even provided unconservative predictions compared with the actual results for cold-formed steel hollow section columns (Meng and Gardner 2020; Ma et al. 2016; Guiaux 1972; Bjorhovde 1977; Braham et al. 1980; Key et al. 1988; Sedlacek et al. 1996; Somodi and Kövesdi 2017). Therefore, the current design provisions are unable to accurately predict the actual capacity of SHS and RHS columns, particularly for high-strength steel and cold-formed steel members. These under- and over-predictions resulting from the existing design provisions indicate the necessity of an accurate prediction model for the buckling capacity of high-strength steel RHS and SHS columns fabricated by different methods.

This study focuses on data analytics in structural engineering and how it helps with incorporating new materials and forming processes into structural steel design. The objectives of this study are: (1) Provide a data structure that includes both experimental and computational data. To this end, the SHS and RHS column buckling capacity was explored in this study. The database includes a wide range of steel grades and geometric properties and both cold-formed and hot-rolled forming processes. Therefore, prediction models based on the database can address the limitations of the current design rules for hollow section columns and additionally provide a way for updating future design specifications. (2) Develop data-driven models using conventional interpolation and newer machine learning algorithms. To that end, a multi-variate linear interpolation model is developed first to examine if enhanced data-driven techniques need to be deployed. (3) Discuss the existing design rules for SHS and RHS capacity estimation. Since the database covers a range of material and geometric properties and formation processes, comparisons between the predictions by the proposed ML models and the current design rules can provide recommendations to improve the design provisions.

2. Design rules for RHS and SHS columns - ANSI/AISC 360-16

Chapter E of the US specification ANSI/AISC 360-16 (2016) provides the design criteria for members under compression. When an SHS and RHS section has a nonslender element that has the width-to-thickness ratio, b/t , of equal or less than $1.4\sqrt{E/F_y}$, where b is width of flat regions and t is thickness (Fig. 1), Eq. 1 is used to derive the design buckling resistance $N_{u,AISC}$ of the section, where F_y is yield strength of material and E is Young's modulus. Cross sections with slender elements, which have b/t greater than $1.4\sqrt{E/F_y}$, should use Eq. 2 which considers an effective cross-sectional area to estimate the buckling resistance:

$$N_{u,AISC} = \phi_c \chi_{AISC} F_y A_g \quad \text{for SHS and RHS with nonslender elements} \quad (1)$$

$$N_{u,AISC} = \phi_c \chi_{AISC} F_y A_e \quad \text{for SHS and RHS with slender elements} \quad (2)$$

where ϕ_c is the resistance factor for compression, equal to 0.9 in AISC 360 2016; A_g is the gross cross-sectional area; A_e is the effective cross-sectional area; χ_{AISC} is the AISC column buckling reduction factor, which can be calculated by either Eq. 3 or Eq. 4 depending on the member slenderness ratio L_c/r or relative slenderness ratio $\lambda_c = (L_c/\pi r)\sqrt{F_y/E}$, in which L_c is the effective member length determined by $KL = L_c$, where K is the effective length factor and L is member length, and r is radius of gyration of a cross section:

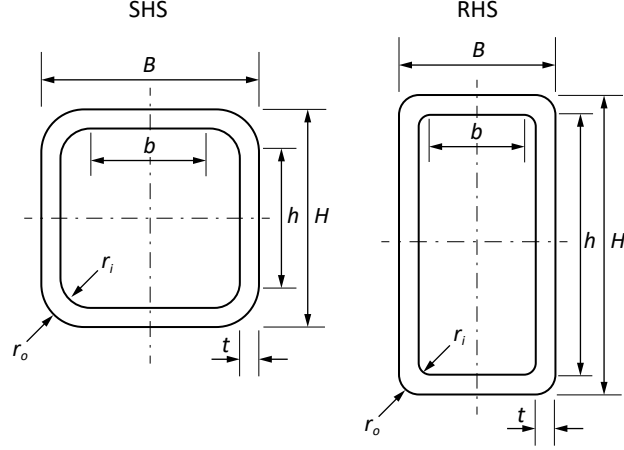


Figure 1: Cross section geometry for SHS and RHS

$$\chi_{AISC} = 0.658 \frac{F_y}{F_e} \quad \text{for } \frac{L_c}{r} \leq 4.71 \sqrt{\frac{E}{F_y}} \quad (\text{or } \lambda_c \leq 1.5) \quad (3)$$

$$\chi_{AISC} = 0.877 \frac{F_e}{F_y} \quad \text{for } \frac{L_c}{r} > 4.71 \sqrt{\frac{E}{F_y}} \quad (\text{or } \lambda_c > 1.5) \quad (4)$$

where F_e is elastic buckling stress, which can be calculated by $(\pi^2 E)/(L_c/r)^2$.

AISC 360 (2016) developed the buckling curve based on columns with an initial out-of-straightness of $L_c/1500$ (Tide 1985; Bjorhovde 1988; Galambos 1998). The buckling curve for hollow sections is applicable to all forming processes and is limited to steel grades up to a yield stress of 485 MPa (70 ksi), however, AISC 360-16 does allow the general use of steel up to 690 MPa (100 ksi) yield stress.

3. Data-driven approaches

As samples in the database are sparsely- and unevenly-scattered, linear multivariate interpolation was implemented to predict the hollow section column buckling capacity for the unsampled locations. In addition, a machine learning algorithm, Multi-layer Perceptron (MLP), was implemented, which has shown success in similar regression tasks for predicting the strength of steel and reinforced concrete structural members and systems (Kim et al. 2021; Kiani et al. 2019; Rahman et al. 2021; Degtyarev 2021). The open-source library *scikit - learn* (2011) in Python 3 was used to implement the algorithms.

3.1 Linear multivariate interpolation

Linear interpolation is a simple mathematical method, involving the generation of new values based on an existing set of values. This method is achieved by rendering linear polynomials to

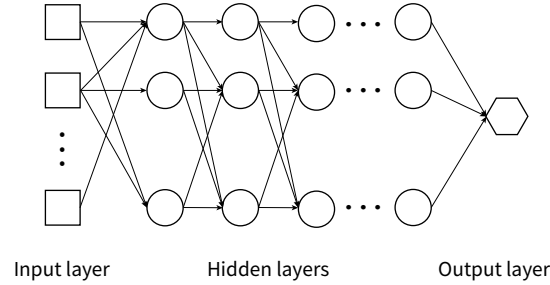


Figure 2: Graphical illustration of multilayer perceptron

construct new data points within the range of a discrete set of known data points. In this study, piecewise-linear interpolation was adopted, which finds interpolated values from meshes created through triangulation of scattered data. This model generates triangles by drawing lines between irregularly gridded data points. Triangle edges are not intersected by each other. The interpolator seems like a patchwork of triangular faces over the extent of the grid. Triangulation with linear interpolation works best when data are evenly distributed over the grid area (Yang et al. 2004).

3.2 Multi-layer perceptron

A multi-layer perceptron (MLP) consists of interconnected neurons transferring information to each other, which is much like the human brain and nerve system, to implement function approximations. The network can be divided into three main layers including an input layer, hidden layers, and an output layer as illustrated in Fig. 2. The input layer is an initial layer of a network that incorporates input variables that will be used to generate an output. The network requires at least one hidden layer which performs computations and operations on the previous layer through a function involving the weights and values in a mathematical form. The weights assigned to the connections between the layers specify the importance of neurons.

4. Database

Data-driven models undergo a training procedure to recognize the patterns in data. Therefore, using reliable training data is crucial for developing an accurate data-driven model. This study established a database of steel SHS and RHS members under compression from the literature including journal papers and technical reports. A total of 695 experimental results (Meng and Gardner 2020; Sedlacek et al. 1999; Ma et al. 2016; Guiaux 1972; BJORHovde 1977; Braham et al. 1980; Key et al. 1988; Somodi and Kövesdi 2017; Rondal 1984; Barber and Birkemoe 1978; Sully and Hancock 1996; Pavlovvcivc et al. 2012; SSAB 2014) and 3,974 FE results (Meng and Gardner 2020) were assembled. Meng and Gardner (2020) developed shell FE models to simulate the buckling test results on hot-rolled and cold-formed steel SHS and RHS columns. Geometrical and material nonlinear analyses with imperfections (GMNIA) were performed in Abaqus (2015). The FE models were validated against the column test results and then utilized in parametric studies with a range of steel grades and geometries to expand the data pool for SHS and RHS column buckling. The detailed FE model description is provided in Meng and Gardner (2020).

Seven input variables that are known to govern the buckling behavior of SHS and RHS members under axial compression were considered, including five geometric parameters, one material property, and formation process. The geometric parameters include four cross-section dimensional properties, such as the overall width B , overall height H , outer corner radius r_o , and thickness t (Fig. 1), and the effective length L_c . Parameters required to calculate the column buckling capacity, such as radius of gyration r , cross-sectional area A , and moment of inertia I were not considered in this section since they can be derived indirectly based on the four cross-section dimensional parameters. For stub columns that are fixed at both ends, the effective length factor K was taken as 0.5. Yield strength F_y is considered a material property. The yield stress of cold-formed steel involves corner strength enhancements that emerge as a result of cold work during production, and appear in cold-formed steel tube sections (Cruise and Gardner 2008; Afshan et al. 2013). This study used the weighted average yield stress given in Eq. 5 to estimate the yield stress of cold-formed steel members incorporating the corner strength enhancements:

$$F_y = CF_{yc} + (1 - C)F_{yf} \quad (5)$$

where F_{yc} is the yield stress of the corner region, F_{yf} is the yield stress of the flat region, and C is the ratio of total corner cross-sectional area to total cross-sectional area of the full section for compression members. Lastly, the forming process was taken into account as an input parameter to develop a consistent prediction model regardless of the manufacturing techniques.

Fig. 3 provides the distribution of the input and output variables grouped by the data source, which are the experimental and FE data, respectively. The histograms include statistical information such as the minimum and maximum values, mean, and coefficient of variation (CV). Histograms with a large CV enable data-driven models to fit a wide range of variables and hence a larger CV is desirable. Comparing the distributions for the experimental and FE data, it can be seen that overall the FE data has a larger density than the experimental data due to its comparatively larger sample size. For some variables that have a significant effect on the buckling capacity as previously discussed in Section 2., the FE data supplements sparse regions of the experimental data. For example, the experimental results focus on yield strength of less than 600 MPa, while the FE data augments the limited samples for high-strength steel columns. Moreover, concerning outer corner radius r_o , thickness t , and the member effective length L_c , the FE data considers larger CVs and adds samples to the database where the experimental data is limited. Distributions for the input features H and B in the FE data are discrete because the FE simulations employed only two values for H and B . Young's modulus E of steel was excluded from the input parameter set due to its minimal variation, which is consistent with the literature (Bartlett et al. 2003; Ellingwood et al. 1982).

Correlation relationships between the input variables and the output variable (N_u) were explored. The correlation coefficient ρ provided in Eq. 6 was utilized to measure a linear correlation:

$$\rho_{X_1, X_2} = \frac{\text{Cov}(X_1, X_2)}{\sigma_{X_1} \sigma_{X_2}} \quad (6)$$

where Cov is the covariance, σ_{X_1} and σ_{X_2} is the standard deviation of input variables X_1 and X_2 ,

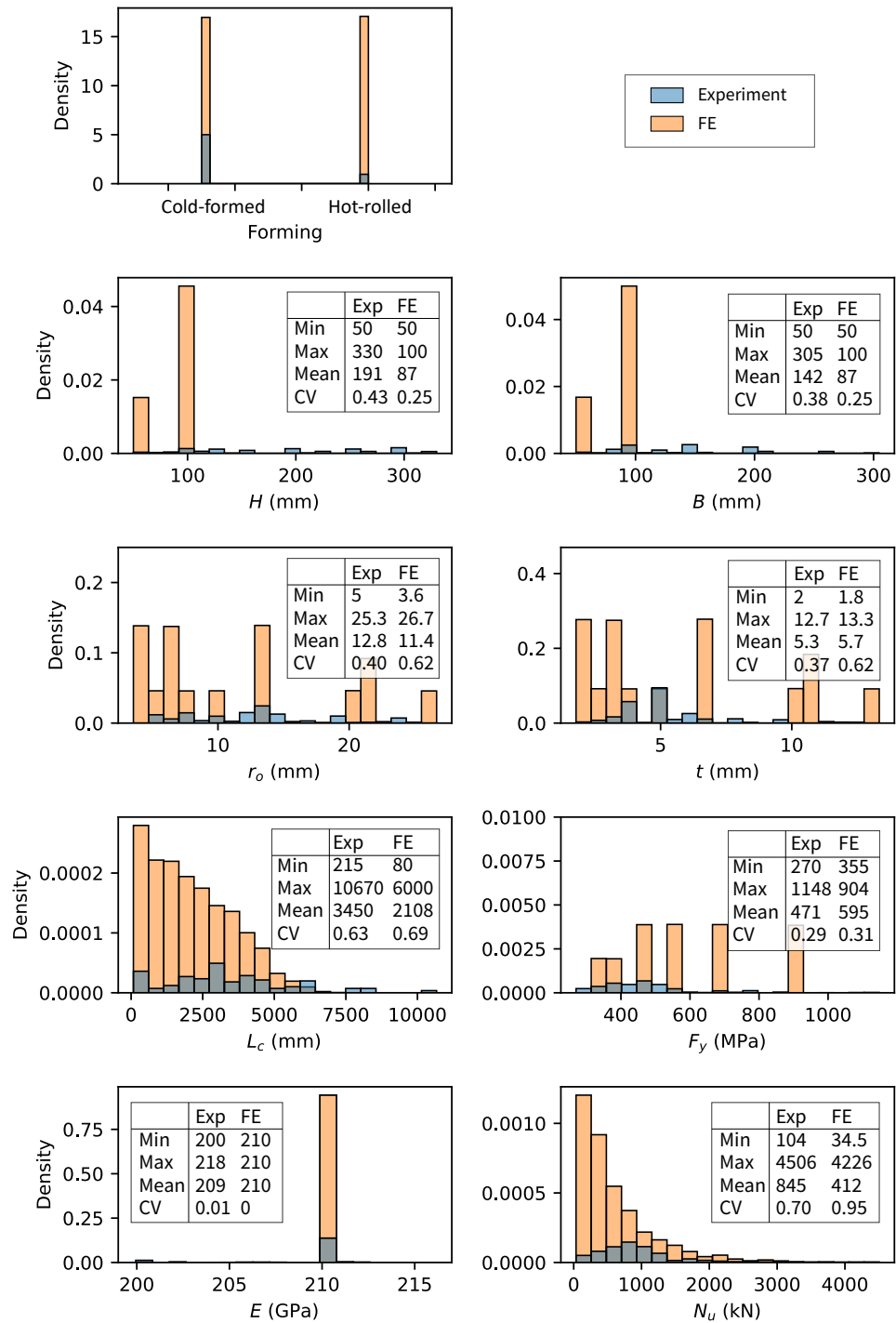


Figure 3: Statistical distributions of the input and output variables

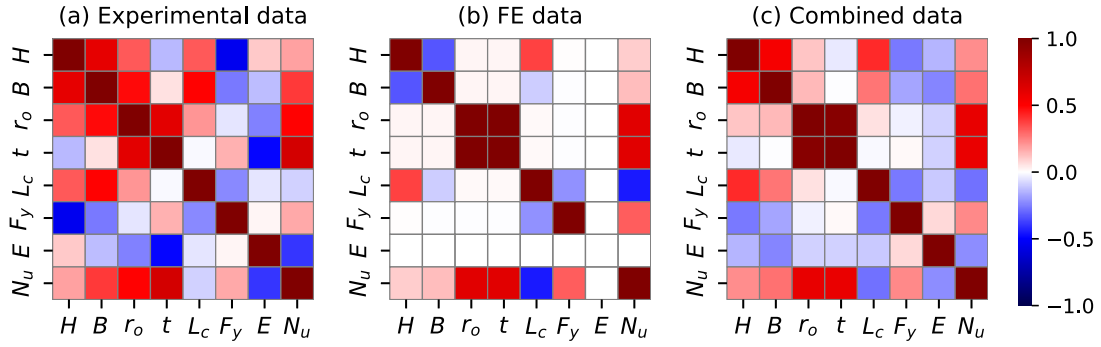


Figure 4: Correlation matrix of the input parameters (a) experimental data (b) FE data (c) combined data

respectively. The coefficient ρ has a range from -1 as the perfect negative correlation to 1 as the perfect positive correlation. When a pair of features have a coefficient close to 1 or -1, the features have a strong relationship. A coefficient of 0 indicates that the two variables are uncorrelated.

Fig. 4 shows the correlation matrix of the variables. The matrix for the experimental data (Fig. 4a) indicates that the response variable N_u is highly correlated only with cross-section thickness with a coefficient value of $\rho = 0.67$. The other input parameters have correlation coefficients lower than 0.5 with the output variable. The buckling capacity N_u in the FE data (Fig. 4b) shows a strong relationship with r_o and t with the same coefficient value of $\rho = 0.61$. It should be noted that those two input features are perfectly correlated with each other according to the FE simulation setup (Meng and Gardner 2020).

The combined data (Fig. 4c) more closely resembles the correlation coefficients for the FE data than the experimental data, which reflects the relatively larger size of the FE data set. For example, the high correlation of B and N_u in the experimental data reduced in the combined data due to the low correlation in the FE data. Comparing the correlation matrices of the experimental and FE data, only the correlation between H and B shows an opposite relationship between the experimental and FE data, which are negative and positive correlations, respectively. As shown in Fig. 3, the FE data included only two different values of B and thus has a small CV and high density, whereas the experimental data has a wider range of the parameter. This large variation in the experimental data led to the combined data having a positive correlation between B and H .

5. Model development

The models were trained on a range of nine data set sizes, from 10% to 90% of the total data, and tested on the remaining data. The data was randomly split into training and test sets. Identical training and testing sets were used for the interpolation and ML algorithms for consistency. A multivariate interpolation model was created in the form of $N_u = f(H, B, r_o, t, L_c, F_y, Forming)$, where the seven input variables were used to approximate the buckling capacity, N_u .

The parameters required by MLP, which is a subset of neural networks and a machine learning

model used in this study, were determined by hyperparameter tuning based on a grid search algorithm with 10-fold cross-validation, which is a technique to search through the best parameter values from a given set of the grid of parameters. It runs through all the different parameters that are fed into the parameter grid and produces the best combination of parameters, based on a scoring metric such as a coefficient of determination. The algorithm evaluates the model performance for each combination to obtain the optimal combination of values from this set. The cross-validation process was performed to reduce errors arising from a random sampling of a training set. During cross-validation, the training set was split into k subsets (folds) and then $k - 1$ subsets were used for model fitting and the remaining subset was used for model validation. A test set was held out for a final evaluation. The model performance from k -fold cross-validation takes an averaged accuracy over k folds, and this study divided the training set into ten folds.

The hyperparameters for the MLP algorithm are as follows: the size of hidden layers was set to (100, 150, 50) in which the first, second, and third hidden layers have 100, 150, and 50 units, respectively; the activation function for the hidden layer was set to the rectified linear activation function ‘ReLU’; the solver for weight optimization was set to ‘lbfgs’ which uses a limited amount of computer memory; the regularization parameter alpha was set to 0.00005; and the learning rate was set to ‘constant’ which adopts a constant learning rate with a step size of 0.001; the maximum number of iterations was set to 1000.

This paper has enabled the analysis models and database to be publicly available on GitHub (<https://github.com/HyeyoungKoh/Data-driven-steel-design>), which is a code hosting platform for version control and collaboration. The analysis methods are coded in Google Colab (short for Collaboratory) for ease of use. The open-source code of the MLP model used in this study will help the stakeholders with understanding the use of data analytics in structural engineering and adopt this modern technology. As all project data have been saved in the accessible repository, future researchers and users can update and modify the codes as needed by accessing the saved version on GitHub.

6. Results

After developing the two data-driven models, the test set was utilized to assess the model performance. The predictive performance was evaluated by estimating the evaluation metrics including the coefficient of determination (R^2) and root mean square error (RMSE), which can be calculated by Eq. 7 and Eq. 8, respectively:

$$R^2 = 1 - \frac{\sum_1^m (y_i - y_{pi})^2}{\sum_1^m (y_i - \frac{1}{m} \sum_1^m y_i)^2} \quad (7)$$

$$\text{RMSE} = \sqrt{\frac{1}{m} \sum_{m=1}^m (y_i - y_{pi})^2} \quad (8)$$

where m is the total number of test data, y_i is the test value, and y_{pi} is the predicted capacity by the prediction models. The R^2 value represents how well the proposed function can predict the test set

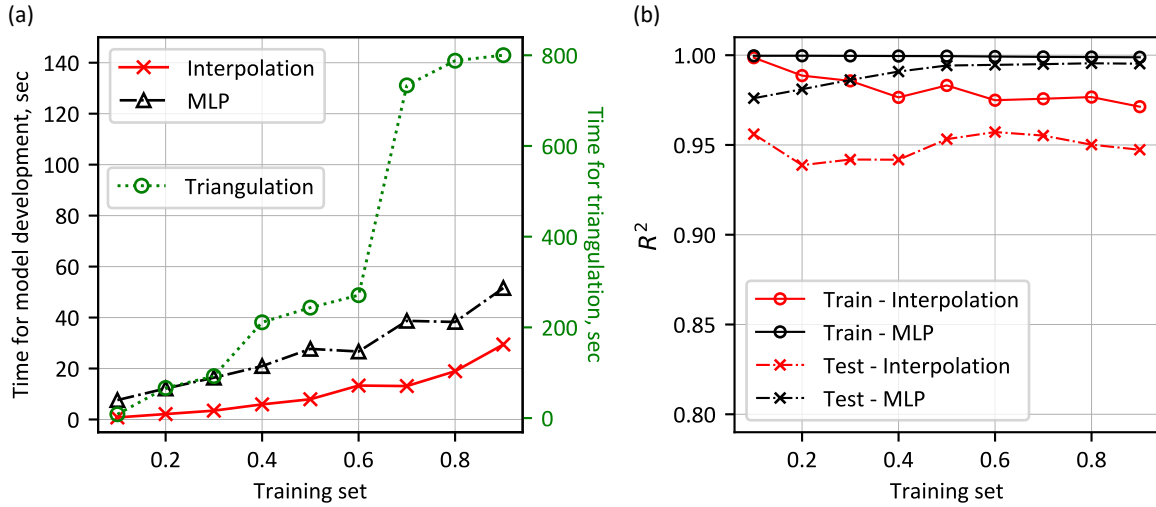


Figure 5: Performance comparison of the data-driven models developed based on the experimental data (a) Computation time (b) computation accuracy

data. The RMSE score quantifies how spread out the prediction errors are, i.e., how concentrated the data is around the line of best fit.

Interpolation and MLP models were developed using a subset of data and tested based on the rest of the data, as detailed in Section 5. Fig. 5a compares the computation time executed for developing the data-driven models. Since the interpolation model requires the process of tessellating triangles in the data, triangulation time is additionally shown. Interpolation has a considerable theoretical foundation in one dimension (Cheney and Light 2009), and it is challenging to implement interpolation when the data size is large while maintaining tractable computational complexity (Lux et al. 2021). Therefore, the time for the triangulation process largely increases as the training set size increases. Although the MLP model demands a higher computational time than the interpolation model with regards to model development, the interpolation model ultimately needs a larger total computational cost. This is because triangulation, which arranges the data for model training, must occur prior to the interpolation model development. When 90% of data was used for model development, the interpolation model demands 16 times the computation time for the MLP model.

Fig. 5b compares the train and test accuracy estimated based on the R^2 score. The performance of the training set is examined in the same method as for the test set in order to check the generalization capacity of the models. This is a common approach when checking the prediction accuracy of ML models. The data-driven models have a higher curve for the training set than the test set because model testing is accomplished using unseen data. Comparing the test performances of the models, the MLP model outperforms the other models with the highest accuracy of 0.995 when 80% of the data is used for training. The interpolation model shows the highest test accuracy only when the training set is 10% of the data. However, the model of this case was developed based on a small sample size, thus the model can be applied to a limited range of parameters. The case of 0.1 is inappropriate to use as a final model because multiple sample sets in the test set can be out of range. According to Fig. 5a and b, it is expected that the interpolation model could lead

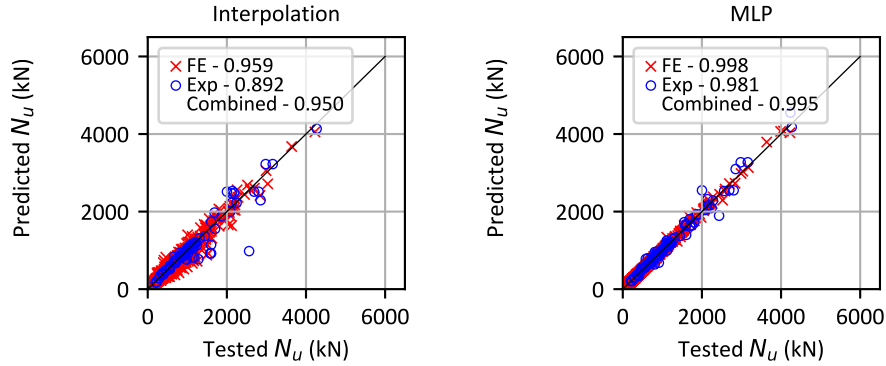


Figure 6: Comparison of the predicted and actual N_u of hollow section columns

to inefficient predictive performance due to its higher computation time and lower accuracy compared with the MLP model. As structural design problems often carry large data, the comparison of computation efficiency and accuracy poses the necessity of implementing enhanced data-driven approaches, i.e., machine learning methods.

Fig. 6 visualizes comparisons of the buckling capacity predicted by the developed models and the actual capacity measured by experiments or FE analyses in the test set. Different train-test splits that showed the best performance in Fig. 5b, 6:4 and 8:2 for the interpolation and MLP models, respectively, were adopted for each model. The coefficients of determination (R^2) are provided separately to assess the performance of the experimental data and FE data. The R^2 value equal to 1.0 represents the perfect prediction. Since the experimental data has a limited sample size compared with the FE data, it showed a lower performance. Comparing the performance of the two models, the MLP model produced a better performance by showing higher R^2 scores, which are 0.998 and 0.981 for the FE and experimental data, respectively. The interpolation model showed the lowest accuracy with scores of 0.959 and 0.892 for FE data and experimental data, respectively. Both models had higher accuracy for the FE data than the experimental data, and the performance of the combined data more closely resembles the R^2 value for the FE data than the experimental data. The lowest accuracy occurred in the experimental data due to its relatively limited sample size in the training set and more inherent uncertainty in the input parameters of physical tests than for FE models. This indicates that the training data should include combined data to cover the entire range of parameters, which might be missing from experimental data only as experiments are typically more limited than FE models but experiments are necessary to validate the FE models.

7. Discussion on the current design rules

This section assesses the proposed ML model by comparing the results to the US codified column buckling design code, AISC 360 (2016), which applies appropriate design equations based on the slenderness of elements and/or members, steel grade, and formation process. In addition, the Specification limits the applicability of the design rules to hollow sections with nominal yield strength only up to 485 MPa. However, the proposed ML method considers a wide range of yield strengths and geometric properties as well as columns manufactured either by cold-forming or

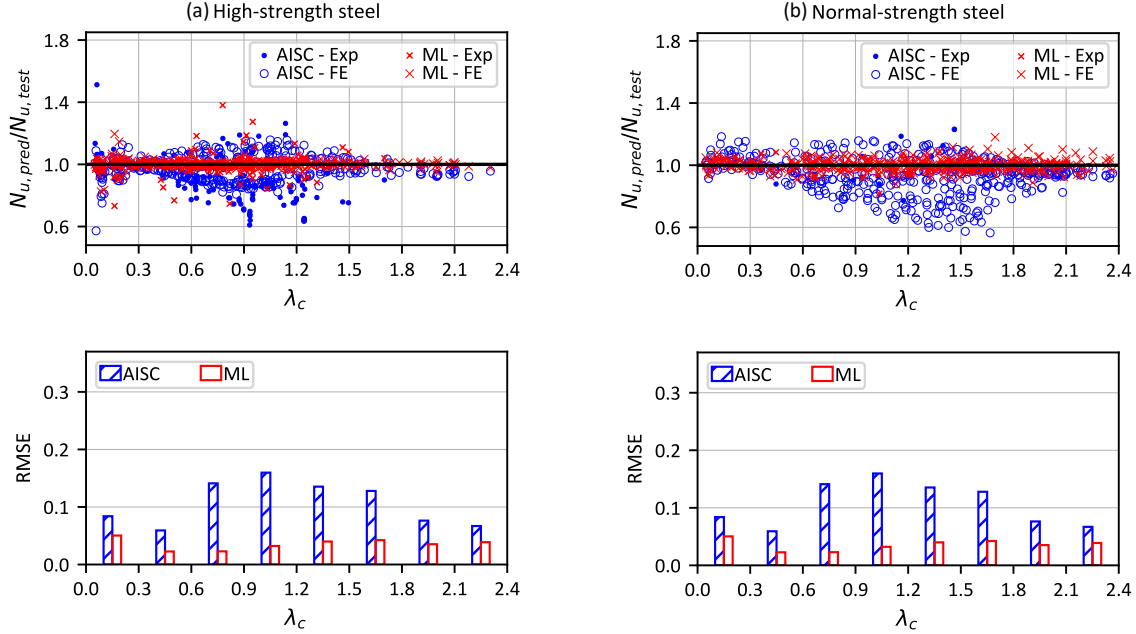


Figure 7: Comparisons of predictions by AISC 360 (2016) and the proposed machine learning model (a) high-strength steel (b) normal-strength steel

hot-rolling, thereby providing a consistent method for estimating the buckling capacity of various tubular section columns.

Fig. 7 compares the prediction-to-test capacity ratios ($N_{u,pred}/N_{u,test}$) derived by the proposed MLP model developed on the train-test split of 8:2 and the current design provisions over the range of the relative member slenderness ratio λ_c . In addition, RMSE for the combined data was measured for the range of λ_c with increments of 0.3. The predicted capacity of the existing design rules was estimated by using the equations that were previously introduced in Section 2. Fig. 7a and b present the comparisons of the data split into two categories, high-strength steel ($F_y \geq 460$ MPa) and normal-strength steel ($F_y < 460$ MPa). Both comparisons show that the existing design rules led to a relatively large scatter band over the entire range of λ_c while the ML results derived a better prediction with a narrow scatter band. The AISC design provision produces large errors for a member in the relative slenderness range between 0.6 and 1.5, which represents the inelastic buckling range where the effects of residual stresses and geometric imperfections are significant. The RMSE plot for high-strength steel predictions again shows that the ML model produces the best accuracy over the entire range of λ_c . It was observed that the AISC model produces more data with lower values of ($N_{u,pred}/N_{u,test}$) for high-strength steel than for normal-strength steel. This is because AISC 360 (2016) applies a single buckling curve which does not capture the influence of the yield strength in the capacity estimation (Meng and Gardner 2020). The proposed ML model demonstrates a high accuracy for both normal- and high-strength steel column predictions.

Fig. 8 compares the predictions generated by the current design provisions and the proposed ML

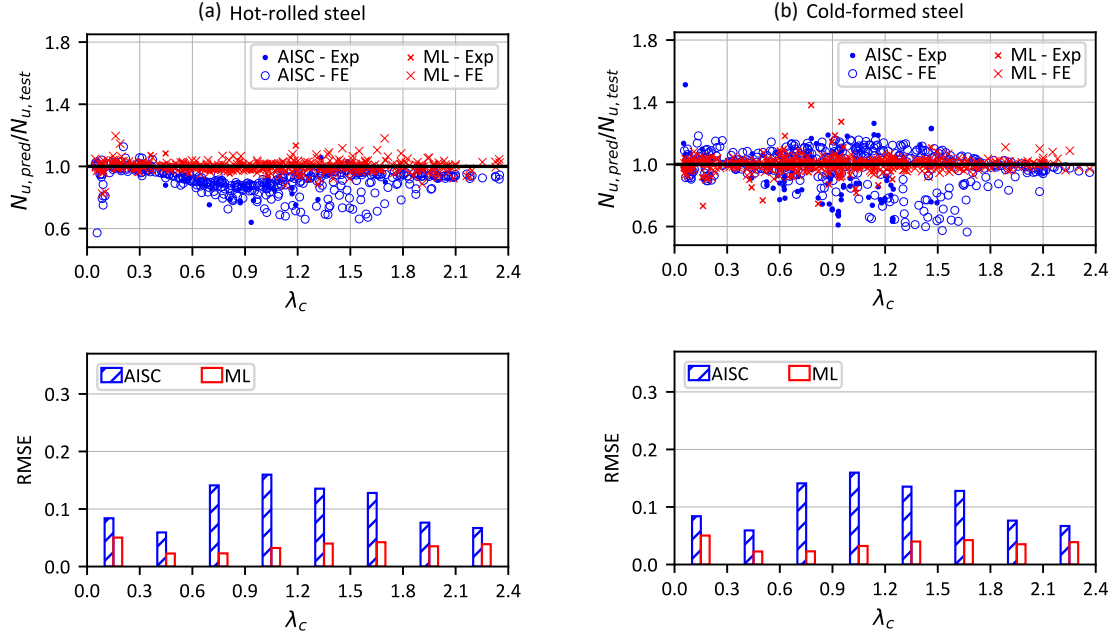


Figure 8: Comparisons of predictions by AISC 360 (2016) and the proposed machine learning model (a) hot-rolled steel (b) cold-formed steel

model by dividing the samples into two groups based on the formation techniques, which are hot-rolled and cold-formed. As shown in Fig. 8a for the hot-rolled steel predictions, the ML model presents better performance by providing a small variance and a low RMSE score than the AISC model. The AISC predictions for hot-rolled steel predominantly appear on the conservative side where $N_{u,pred}/N_{u,test} \leq 1.0$ with a wide scatter band and thereby a larger error (RSME). For the cold-formed steel results (Fig. 8b), however, a large number of the AISC predictions occurred in the unconservative zone, where the capacity ratio is greater than 1.0. This indicates that formation methods have a significant effect on the capacity if the physics-based model is used. It should be noted that AISC 360 (2016) does not reflect the different buckling capacities between formation techniques. The provided comparisons between the proposed ML model and the current design method in this section demonstrate the consistency and good performance of the proposed ML model for predicting both hot-rolled and cold-formed column capacities over the range of the relative slenderness ratio λ_c .

8. Conclusions

This paper presented data-driven models for buckling capacity prediction of square and rectangular hollow section (SHS and RHS) members under compression, which are manufactured by cold-forming or hot-rolling and composed of high-strength or normal-strength steel. Linear interpolation and multilayer perceptron (MLP) models were developed on a database of previously published 695 experimental results and 3,794 finite element (FE) analysis results of SHS and RHS columns. The columns in the database covered a wide range of material and geometric properties

such as steel grades, cross-sectional dimensions, and member slenderness. Triangulation was performed to create meshes from the data for interpolation model development. The MLP model was optimized by performing feature scaling, hyperparameter tuning, and cross-validation. The two developed data-driven models were evaluated by computation time and accuracy. Finally, the best model was further verified by the comparisons with the existing design rules for columns provided in AISC 360-16. The significant findings of this research are summarized in the following:

- Computation time and accuracy of the two data-driven models demonstrated the advantages of the machine learning model. As the conventional interpolation model needed time for creating meshes from the discrete data, a large amount of time was executed for developing the interpolation model. Additionally, the accuracy estimated by the coefficient of determination R^2 was lower in the interpolation model compared with the machine learning model.
- The developed data-driven models were separately evaluated based on the data groups: (1) experimental data only, (2) FE data only, and (3) combined data. For both the interpolation and MLP models, the performance on the FE data was the highest among the three data groups.
- The database and models are publicly available on the GitHub repository, <https://github.com/HyeyoungKoh/Data-driven-steel-design>. They are coded in a computational notebook format, which can be executed through the web browser without configuration and installation of software on a local server. Future researchers can update and modify the codes and database as needed.
- The developed MLP model, which showed better performance than the interpolation model, was further evaluated by comparing to the predictions obtained from the existing design rules in AISC 360-16 for SHS and RHS columns. The ratios of predicted-to-tested capacity derived from AISC 360 and the proposed MLP model were compared. The comparisons were separately implemented on (1) normal- and high-strength steel columns and (2) hot-rolled and cold-formed columns. The MLP model demonstrated a consistent performance, which provided the capacity ratio close to 1.0 with a small variance, over the entire range of the member slenderness ratio and across different steel grades and forming techniques, whereas the existing design methods showed inconsistent performance with relatively large root mean squared errors and variance.

The consistency and high performance of the proposed ML model indicates that machine learning based design can be a viable method for the accurate prediction of SHS and RHS column capacity. This could augment design provisions which may not directly reflect the importance of all properties such as high-strength steel or specific manufacturing process.

References

Abambres, M. et al. (2018). “Neural Network-based formula for the buckling load prediction of I-section cellular steel beams”. *Comput* 8.1, p. 2.

- Afshan, S., B. Rossi, and L. Gardner (2013). “Strength enhancements in cold-formed structural sections—Part I: Material testing”. *J Constr Steel Res* 83, pp. 177–188.
- American Institute of Steel Construction (2016). *Specification for Structural Steel Buildings*. Chicago, IL: ANSI/AISC 360-16.
- AS 4100 (1998). *Steel Structures*. Sydney, Australia: Standards Australia.
- AS/NZS 4600 (2018). *Cold-Formed Steel Structures*. Standards Australia.
- Barber, J. D. and P. C. Birkemoe (1978). *An experimental investigation of the column behaviour of cold-formed stress-relieved hollow structural steel sections*. Department of Civil Engineering, University of Toronto.
- Bartlett, F. M. et al. (2003). “Updating standard shape material properties database for design and reliability”. *Eng J AISC* 40.1, pp. 2–14.
- Bjorhovde, R. (1977). *Strength and behavior of cold-formed HSS columns*. Tech. rep. Rep. No. 65. Edmonton, AB, Canada: Univ. of Alberta.
- Bjorhovde, R. (1988). “Columns—from theory to practice”. *ENG J-AISC* 25.1, pp. 21–34.
- Braham, M. et al. (1980). *Flambement des profils creux a parois minces. Cas des profils rectangulaires charges axialment*. Tech. rep. CIDECT 2H 79/19. Altendorf, Switzerland: Committee for International Development and Education on Construction of Tubular Structures.
- Cheney, E. W. and W. A. Light (2009). *A course in approximation theory*. Vol. 101. American Mathematical Soc.
- Cruise, R. B. and L. Gardner (2008). “Strength enhancements induced during cold forming of stainless steel sections”. *J Constr Steel Res* 64.11, pp. 1310–1316.
- CSA S16:19 (2019). *Design of Steel Structures*. Toronto, Ontario, Canada: Canadian Standards Association.
- Dai, Y. et al. (2022). “A novel machine learning model to predict the moment capacity of cold-formed steel channel beams with edge-stiffened and un-stiffened web holes”. *J Build Eng* 53, p. 104592.
- El-Dakhkhni, W. (2021). “Data analytics in structural engineering”. DOI: 10.1061/(ASCE)ST.1943-541X.0003112.
- Dassault Systems (2015). *Abaqus/CAE*. Johnston, RI: Dassault Systems: V6.16.
- Degtyarev, V. V. (2021). “Neural networks for predicting shear strength of CFS channels with slotted webs”. *J Constr Steel Res* 177, p. 106443.
- Ellingwood, B. et al. (1982). “Probability based load criteria: load factors and load combinations”. *J Struct Div* 108.5, pp. 978–997.
- European Committee for Standardization (2014). *Eurocode 3—Design of steel structures—Part 1-1: General rules and rules for buildings*. Brussels, Belgium: EN 1993-1-1.
- Fang, Z. et al. (2021). “Deep learning-based procedure for structural design of cold-formed steel channel sections with edge-stiffened and un-stiffened holes under axial compression”. *Thin-Walled Struct* 166, p. 108076.
- Galambos, T. V. (1998). *Guide to stability design criteria for metal structures*. 5th ed. John Wiley & Sons.
- Guiaux, P (1972). *Essais de flambement sur profils creux formes a froid, carres et circulaires*. Tech. rep. Altendorf, Switzerland: CIDECT 72/28/F.
- Key, P. W., S. W. Hasan, and G. J. Hancock (1988). “Column behavior of cold-formed hollow sections”. *J Struct Eng* 114.2, pp. 390–407.

- Kiani, J., C. Camp, and S. Pezeshk (2019). “On the application of machine learning techniques to derive seismic fragility curves”. *Comput Struct* 218, pp. 108–122.
- Kim, S. H. et al. (2021). “Strength prediction of steel CHS X-joints via leveraging finite element method and machine learning solutions”. *J Constr Steel Res* 176, p. 106394.
- Kumar, M. and N. Yadav (2013). “Buckling analysis of a beam–column using multilayer perceptron neural network technique”. *J Franklin Inst* 350.10, pp. 3188–3204.
- Lux, T. C. H. et al. (2021). “Interpolation of sparse high-dimensional data”. *Numer Algorithms* 88.1, pp. 281–313.
- Ma, J. L., T. M. Chan, and B. Young (2016). “Experimental investigation on stub-column behavior of cold-formed high-strength steel tubular sections”. *J Struct Eng* 142.5, p. 04015174.
- Meng, Xin and Leroy Gardner (2020). “Behavior and design of normal-and high-strength steel SHS and RHS columns”. *J Struct Eng* 146.11, p. 04020227.
- Pala, M. (2006). “A new formulation for distortional buckling stress in cold-formed steel members”. *J Constr Steel Res* 62.7, pp. 716–722.
- Pavlovčič, L. et al. (2012). “Finite element simulation of slender thin-walled box columns by implementing real initial conditions”. *Adv Eng Softw* 44.1, pp. 63–74.
- Pedregosa, F. et al. (2011). “Scikit-learn: Machine learning in Python”. *the Journal of machine Learning research* 12, pp. 2825–2830.
- Pu, Y. and E. Mesbahi (2006). “Application of artificial neural networks to evaluation of ultimate strength of steel panels”. *Eng Struct* 28.8, pp. 1190–1196.
- Rahman, J. et al. (2021). “Data-driven shear strength prediction of steel fiber reinforced concrete beams using machine learning approach”. *Eng Struct* 233, p. 111743.
- Rondal, J (1984). “Contribution à l’étude de la stabilité des profils creux à parois minces”. PhD thesis. Université de Liège, Faculté des sciences appliquées.
- Sedlacek, G, B Kuhn, et al. (1999). *Buckling behaviour of hot-formed SHS in high strength steel grade E-460*. Tech. rep. Altendorf, Switzerland: Comite international pour le developpement et l’etude de la construction tubulaire, Cidect report 2T-2/99.
- Sedlacek, G, J Rondal, et al. (1996). *Buckling behaviour of a new generation of cold formed hollow sections*. Tech. rep. Aachen University, Aachen, Germany: Final CIDECT report 2R-2/96.
- Sheidaii, M. R. and R. Bahraminejad (2012). “Evaluation of compression member buckling and post-buckling behavior using artificial neural network”. *J Constr Steel Res* 70, pp. 71–77.
- Somodi, B and B Kövesdi (2017). “Flexural buckling resistance of cold-formed HSS hollow section members”. *J Constr Steel Res* 128, pp. 179–192.
- SSAB (2014). *Axial resistance of double grade (S355, S420) hollow sections manufactured by SSAB, statistical evaluation based on tests*. Tech. rep. Helsinki, Finland.
- Sully, R. M. and G. J. Hancock (1996). “Behavior of cold-formed SHS beam-columns”. *J Struct Eng* 122.3, pp. 326–336.
- Tide, R. H. R. (1985). “Reasonable column design equations”. *Proceedings 1985 Annual Technical Session*. Bethlehem, PA: Structural Stability Research Council.
- Wang, J. and L. Gardner (2017). “Flexural buckling of hot-finished high-strength steel SHS and RHS columns”. *J Struct Eng* 143.6, p. 04017028.
- Xu, Y., B. Zheng, and M. Zhang (2021). “Capacity prediction of cold-formed stainless steel tubular columns using machine learning methods”. *J Constr Steel Res* 182, p. 106682.
- Yang, C. S. et al. (2004). “Twelve different interpolation methods: A case study of Surfer 8.0”. *Proceedings of the XXth ISPRS congress*. Vol. 35, pp. 778–785.